Using Demand Response to Shape the Fast Dynamics of the Bulk Power Network

Kasra Koorehdavoudi*
School of Electrical Engineering & Computer Science
Washington State University
Pullman, WA, USA
Email: kkoorehd@eecs.wsu.edu

Mengqi Yao* and Johanna L. Mathieu
Department of Electrical Engineering & Computer Science
University of Michigan
Ann Arbor, MI, USA
Email: {mqyao, jlmath}@umich.edu

Sandip Roy
School of Electrical Engineering & Computer Science
Washington State University
Pullman, WA, USA
Email: sroy@eecs.wsu.edu

***Abstract*—Demand-side strategies for shaping the fast dynamics of the bulk power transmission network are explored. Specifically, the design of demand response strategies is pursued, with the aim of modulating the network's operating point so as to achieve desirable small-signal characteristics. The design problem is posed as an optimization problem wherein the total demand responsive load is held constant but shifted between different buses, to maximize a performance metric which captures disturbance susceptibility and control-channel performance. The problem is solved numerically with an iterative linear programming algorithm that uses eigenvalue sensitivity analysis and linearizations of the nonlinear constraints. Formal characterization of the optimal solution is also explored. A small-scale case study using the Kundur 11-bus two-area test system demonstrates that, by shifting the load between two areas, the smallest damping ratio of the generator modes (corresponding to the disturbance susceptibilty) and the smallest damping ratio of the finite zeros of the input-output transfer function (corresponding to the control channel performance) can be improved. The improvements due to load shifting are compared to those possible with generator re-dispatch and voltage regulation.**

***Index Terms*—demand response, optimization, eigenvalue sensitivity, smallest damping ratio, power system stability**

I. Introduction

Small-signal and transient characteristics of the bulk power transmission network are strongly modulated by the operating point of the network. While an array of fast controls are in place that ensure stability and sufficient damping across typical operating conditions, the high penetration of intermittent renewables in many power systems is causing deviations away from typical operating points, and introducing far greater variability in the operating points. In some networks, increasing demand and isolation of generation from load centers (e.g., offshore wind farms) are also leading to highly stressed (highly loaded or congested) operating points. At the same time, power networks are being subject to an increasing diversity of disturbances that can initiate fast dynamics, as new cyber-enabled technologies are integrated, distribution systems become more complex, and control paradigms change. There is a growing concern that these changes together may cause the transmission network to be increasingly vulnerable to wide-area oscillations or even destabilization.

The operating point of the power network can be shaped to ensure that the network's small-signal and transient responses are desirable [1], [2]. Indeed, today's economic dispatch procedures implicitly account for transient and small-signal characteristics, by imposing a stability constraint or margin on the optimal power flow solution. These designs guarantee stability under nominal conditions and also for any single-component failure, provided that the models for fast dynamics are accurate. However, the constraint-based solutions may not be appealing if variability in renewable generation persistently requires alteration of dispatch to maintain stability, given the possible high economic costs of modifying dispatch. Also, stability-constrained economic dispatch does not consider refined shaping of the fast dynamics (e.g., design of damping or disturbance-response properties), nor account for for the dynamics of existing fast controls in the network.

With this motivation, some studies have considered tuning of dispatch to increase damping or stability margins. Kundur and co-authors have addressed generator re-scheduling to increase power transfer while continuing to adhere to a small-signal stability constraint, using a sensitivity-based approach [3]. Several studies have sought to improve damping ratios of inter-area modes via re-dispatch, whether based on a formal analysis/optimization [3], [4], [5] or from data obtained from wide-area measurement systems [6]. Load reduction in addition to generator re-dispatch to reduce flows on tie-lines has also been considered in [7], with the aim of improving inter-area mode damping. Meanwhile, [8] differentiated critical versus non-critical machines to achieve re-dispatch to satisfy specified transient stability margins. These techniques can support re-dispatch in response to an observed transient stability concern, but are limited by generator ramping constraints and high dispatch costs.

In this study, demand-side strategies for reshaping the small-signal characteristics of the network are explored. Demand response and other load controls are becoming increasingly practical [9], providing further degrees of flexibility as compared to generator re-dispatch. Additionally, loads may be able to respond faster and/or more cost-effectively than generators.

*The first two authors contributed equally to this work. This research was supported by NSF Awards #1549670, #1545104, and #1635184.

Thus, demand-side solutions may prove useful to improve transient and small-signal charactistics at both the time of unit commitment and economic dispatch, and at shorter time horizons (e.g. 5-10 minutes) when small-signal or transient stability concerns are detected. The focus of this study is on re-dispatch at shorter time horizons using spatial load shifting that keeps total load constant so as not to affect the system frequency. The re-dispatch problem is posed as a optimization problem, wherein loads are designed within constraints to improve 1) wide-area oscillatory responses, and 2) control channel characteristics. Numerical techniques for optimization as well as simple graph-theoretic insights into the optimal solution are pursued.

Demand response has already been envisioned as a tool to support power system security, broadly defined. In particular, demand response has been used to provide frequency regulation, improving frequency stability [10], [11]. In that line of research, the goal is to shift demand in time to either match a scaled automatic generation control signal or respond to locally-measured frequency deviations. Demand can also be shifted spatially to improve power system voltage stability. For example, [12] proposes an algorithm that shifts load between buses, while maintaining a constant total load, to improve measures of static voltage stability, including the smallest singular value of the power flow Jacobian and the loading margin (i.e., the amount of load that can be added to the system before power flow becomes infeasible). Since the total load is constant, the total generation is constant (other than that needed to compensate the change in system losses) and so the frequency is unaffected. Such a strategy could be used if the system is operating close to its feasibility limits and generators are unable to respond sufficiently-quickly to correct the problem. Fast-acting demand responsive loads would respond initially until the generators can take over. In contrast, few techniques have been established to use demand response to enhance dynamic (small signal, transient) stability, although the problem has been considered in a couple of very recent studies [13]. Our work contributes to the effort to exploit demand response to enhance dynamic stability of the bulk power system.

Relative to previous studies, the main contribution of this work is a methodology for the systematic design of spatial load shifts to shape the fast dynamics of the power transmission network. Specifically, an optimization framework is developed to maximize the weighted sum of several performance metrics corresponding to small-signal stability and control channel performance. Case studies show that load-side solutions can achieve meaningful improvements in small-signal performance, although load and generation co-design is more effective.

This paper is structured as follows. A conceptual description of the problem is given in Section II. Mathematical descriptions of the power-system model, performance metrics, and optimization problem are given in Section III. In Section IV, an approach for solving the optimization problem numerically is described. In Section V, insights into the system characteristics at the optimum are presented. Case studies are dveloped in Section VI, and finally brief conclusions are given in Section VII.

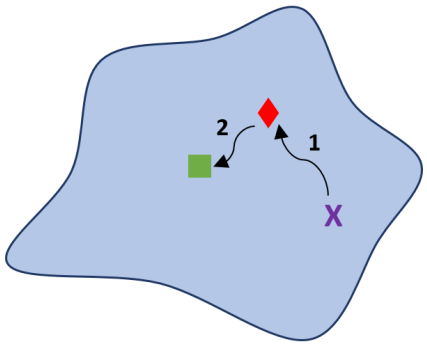

Fig. 1. Conceptual illustration of the problem. The blue area is the (non-convex) stability region. The purple cross is the initial operating point. The red diamond is the operating point after a demand response action. The green square is the operating point after the generators take over.

II. Problem Description

Demand response actions influence the static and dynamic characteristics of the transmission network by modifying loading profiles across the network. While the traditional motivation for using demand response is market-related, load shifting/shedding can also be used by system operators to alleviate congestion or otherwise alter the operating point in desirable ways. Relevant to our efforts here, spatial load shifts may improve the small-signal and transient response characteristics in several ways: 1) by increasing the transient stability margin of the network, 2) by decreasing the sensitivity (equivalently, increasing the resiliency) of the network to possible disturbances, and 3) by shaping control channel characteristics so that implemented controls can appropriately handle disruptions. We pose the problem as an optimization problem, wherein demand responsive loads are tuned (increased/decreased) to optimize a performance function that combines these three goals. The total demand responsive load is constrained to be constant. We assume generator outputs have been determined previously via the unit commitment and economic dispatch algorithms and that they are fixed over the time frame of interest, with the exception of the reference generator, which compensates for the change in system losses resulting from the change in load pattern.

A conceptual illustration of the problem is shown in Fig. 1. The shaded region is the stability region. The initial operating point is shown with the purple cross. The system operator would like to increase the stability margin(s) of the system by increasing/decreasing fast-acting demand responsive loads (step 1), resulting in a new operating point, shown with the red diamond. Next, the system operator would re-dispatch (slower) generation to both maintain/improve the new stability margins and compensate the demand response actions (step 2), i.e., loads that consumed more/less than their baseline in step 1, now need to consume less/more than their baseline to ensure they receive their desired amount of energy over the

full interval, resulting in a new operating point, shown with the green square. Here we focus on step 1 and leave step 2 for future work.

III. Problem Formulation

A. Notation

Variables & Parameters

θ_i	Voltage angle at bus i
V_i	Voltage magnitude at bus i
$\underline{V}_i$, $\overline{V}_i$	Min/Max voltage magnitude at bus i
δ_i	Electrical angle of generator i
δ_i^{ss}	Steady-state electrical angle of generator i
ω_i	Frequency of generator i
E_i^{ss}	Steady-state emf magnitude of generator i
p_i	Real power injection at bus i
$p_{g,i}$	Real power generation at bus i
$p_{m,i}$	Mechanical power at generator i
$\underline{p}_i$, $\overline{p}_i$	Min/Max real power injection at bus i
q_i	Reactive power injection at bus i
$q_{g,i}$	Reactive power generation at bus i
$\underline{q}_i$, $\overline{q}_i$	Min/Max reactive power injection at bus i
n	Number of buses
m	Number of generators
G_{ij}	Conductance of line ij
B_{ij}	Susceptance of line ij
x_i'	Transient reactance of generator at bus i
H_i	Inertia of generator i
D_i	Damping of generator i
Y	Bus admittance matrix
$\bar{Y}$	Reduced admittance matrix
$\bar{G}_{ij}$	Real part of $\bar{Y}_{ij}$
$\bar{\phi}_{ij}$	Phase angle of $\bar{Y}_{ij}$
$\tilde{Y}$	Augmented admittance matrix
L	Laplacian matrix
ε_0	Total demand responsive load
μ_i	Ratio of real and reactive demand at bus i
λ	Eigenvalue of a matrix
α	Real part of an eigenvalue
β	Imaginary part of an eigenvalue
η	Damping ratio of an eigenvalue
u	Normalized right eigenvector
w	Normalized left eigenvector
γ	Weighting factor
A, B, C	Linear system matrices
$\mathbf{x}$	Linear system state vector

Functions

$\mathcal{F}_i^P(\cdot)$	Real power injection at bus i
$\mathcal{F}_i^Q(\cdot)$	Reactive power injection at bus i
$\mathcal{G}_i^E(\cdot)$	emf magnitude of generator i
$\mathcal{G}_i^\delta(\cdot)$	Electrical angle of generator i
$f_i^P(\cdot)$	Linearization of $\mathcal{F}_i^P$
$f_i^Q(\cdot)$	Linearization of $\mathcal{F}_i^Q$
$g_i^E(\cdot)$	Linearization of $\mathcal{G}_i^E$
$g_i^\delta(\cdot)$	Linearization of $\mathcal{G}_i^\delta$
$\mathcal{H}(\cdot)$	Reduced admittance matrix

Sets

$\mathcal{N}$	Set of all buses
$\mathcal{S}_{\mathrm{PV}}$	Set of all PV buses
$\mathcal{S}_{\mathrm{PQ}}$	Set of all PQ buses
$\mathcal{S}_{\mathrm{DR}}$	Set of buses with demand responsive loads
$\mathcal{S}_{\mathrm{G}}$	Set of generators

Bold symbols denote vectors including all variables of a type. Subscript 'ref' denotes the slack bus. Superscript '0' denotes the current operating point, and superscript '$*$' denotes the optimal solution of the problem. The function eig $(\cdot)$ takes the eigenvalues of the matrix.

B. Power System Model

We consider a bulk power transmission system with n buses, labeled $1, \ldots, n$, belonging to set $\mathcal{N}$. A subset of the buses, labeled $1, \ldots, m$, have inertial generation associated with them. One is modeled as a slack bus while the others are modeled as PV buses belonging to set $\mathcal{S}_{\mathrm{PV}}$. A second subset are load-only and are modeled as PQ buses belonging to set $\mathcal{S}_{\mathrm{PQ}}$. Of the PQ buses, a portion contain demand responsive loads and belong to set $\mathcal{S}_{\mathrm{DR}}$. The bus admittance matrix is denoted by Y. The nominal operating point of the network, prior to deployment of demand response, is specified by the quadruple of vectors $(\boldsymbol{p^0}, \boldsymbol{q^0}, \boldsymbol{V^0}, \boldsymbol{\theta^0})$, which indicate the real power, reactive power, voltage, and voltage angle at the buses. The nominal operating point typically would be determined in advance via an economic dispatch algorithm.

We assume the real power consumption of demand responsive loads can be increased/decreased within certain limits. Formally, the $n \times 1$ vector $\boldsymbol{p}$ specifies the modified real power injection at each bus after the demand response actions have been taken. Our goal is to design $\boldsymbol{p}$ to shape small-signal characteristics of the network, subject to constraints on the amount of load increase/decrease allowed at each bus with demand responsive loads and on the total load, which we constrain to remain to unchanged from the nominal. This can be captured with the following constraints: $\underline{p}_i \leq p_i \leq \overline{p}_i$, $\forall i \in \mathcal{S}_{DR}$ and $\sum_{i \in \mathcal{S}_{DR}} p_i = \varepsilon_0$, where ε_0 is the total demand responsive load. The real power injections and voltage magnitudes of the PV buses are assumed unchanged from the nominal (i.e., $p_i = p_i^0$, $V_i = V_i^0, \forall i \in \mathcal{S}_{\mathrm{PV}}$), as are the voltage magnitude and phase at the slack bus (i.e., $V_{\mathrm{ref}} = V_{\mathrm{ref}}^0$, $\theta_{\mathrm{ref}} = 0$). The voltage magnitudes at the PQ buses are constrained within reasonable limits. In addition, the ratio of the real and reactive demand at each PQ bus is assumed fixed (i.e., $p_i \cdot \mu_i = q_i, \forall i \in \mathcal{S}_{\mathrm{PQ}}$, where μ_i is a constant).

The change in the real power vector changes the operating point of the power system. The standard AC power flow equations [14] are solved to find the new operating point $(\boldsymbol{p}, \boldsymbol{q}, \boldsymbol{V}, \boldsymbol{\theta})$, specifically,

$$p_i = \mathcal{F}_i^P(\boldsymbol{\theta}, \boldsymbol{V}), \tag{1}$$

$$q_i = \mathcal{F}_i^Q(\boldsymbol{\theta}, \boldsymbol{V}), \tag{2}$$

where $\mathcal{F}_i^P(\boldsymbol{\theta}, \boldsymbol{V}) = V_i \sum_{j \in \mathcal{N}} V_j (G_{ij} \cos(\theta_i - \theta_j) + B_{ij} \sin(\theta_i - \theta_j))$ and $\mathcal{F}_i^Q(\boldsymbol{\theta}, \boldsymbol{V}) = V_i \sum_{j \in \mathcal{N}} V_j (G_{ij} \sin(\theta_i - \theta_j)$

$-B_{ij}\cos(\theta_i-\theta_j))$, where $G_{ij} = \mathrm{Re}(Y_{ij})$ and $B_{ij} = \mathrm{Im}(Y_{ij})$. The real and reactive power injections are known (or optimized) for the PQ buses, while the real power injection and voltage magnitude are known (or optimized) for the PV buses; the remaining $2n$ variables are found from the equations.

The system contains m generators belong to set $\mathcal{S}_{\mathrm{G}}$. The steady state emf magnitude of generator i is

$$E_i^{ss} = \mathcal{G}_i^E(\boldsymbol{\theta}, \boldsymbol{V}) = \left| V_i\angle\theta_i + x_i' \frac{p_{g,i} - jq_{g,i}}{V_i\angle -\theta_i} \right|, \qquad (3)$$

where $p_{g,i}$ and $q_{g,i}$ are the real and reactive power generation at generator i, and x_i' is the transient reactance of generator i. The steady state electrical angle (relative to a reference angle) of generator i is

$$\delta_i^{ss} = \mathcal{G}_i^\delta(\boldsymbol{\theta}, \boldsymbol{V}) = \angle\left(V_i\angle\theta_i + x_i' \frac{p_{g,i} - jq_{g,i}}{V_i\angle -\theta_i} \right). \qquad (4)$$

Note that the superscript ss is used to denote steady state values to prevent the confusion with transient values.

We are interested in designing the small-signal characteristics of the power system, which are based on the swing dynamics of the network. In particular, power-system transients are analyzed via the nonlinear swing equations, with small-signal characteristics being extracted from their linearizations around the operating point. Here, the classical nonlinear swing dynamics model [15] is used. In this model, the electrical angle δ_i of each generator is governed by:

$$\begin{aligned} H_i\ddot{\delta}_i =& p_{g,i} - D_i\dot{\delta}_i - (E_i^{ss})^2\bar{G}_{ii} \\ & - \sum_{j\neq i} E_i^{ss}E_j^{ss}|\bar{Y}_{ij}|\cos\big(\delta_i - \delta_j - \bar{\phi}_{ij}\big), \end{aligned} \qquad (5)$$

where H_i and D_i are the inertia and damping, respectively, of generator i. Also, $\bar{G}_{ij}$, $|\bar{Y}_{ij}|$, and $\bar{\phi}_{ij}$ are the real part, magnitude, and phase angle, respectively, of $\bar{Y}_{ij}$, where $\bar{Y} = \mathcal{H}(Y, \boldsymbol{p})$ is the reduced admittance matrix. To compute $\bar{Y}$, Y is first augmented to capture loads as fixed admittances and to include the generator internal nodes as new buses. The augmented matrix $\widetilde{Y}$ is partitioned to separate the generator internal nodes from the remaining nodes, as $\widetilde{Y} = \begin{bmatrix} \widetilde{Y}_{gg} & \widetilde{Y}_{gl} \\ \widetilde{Y}_{lg} & \widetilde{Y}_{ll} \end{bmatrix}$, where $\widetilde{Y}_{gg}$ corresponds to the generator internal nodes (which are listed first without loss of generality). Then the reduced admittance matrix is found as $\bar{Y} = \widetilde{Y}_{gg} - \widetilde{Y}_{gl}\widetilde{Y}_{ll}^{-1}\widetilde{Y}_{lg}$.

The design variables $\boldsymbol{p}$ modify the nonlinear swing equations by changing $\boldsymbol{\delta}^{ss}$, $\boldsymbol{E}^{ss}$, and $\bar{Y}$, specifically $\boldsymbol{\delta}^{ss}$ and $\boldsymbol{E}^{ss}$ change as a result of the change in the power flow and $\bar{Y}$ changes as the result of the change in load model (i.e., from constant power to constant impedance). If the transient reactance of generator is small, the steady-state phase angles $\boldsymbol{\theta}$ are an equilibrium solution for the electrical angles $\boldsymbol{\delta}$.

Linearizing the nonlinear swing equations around the operating point yields the following model:

$$\underbrace{\begin{bmatrix} \dot{\boldsymbol{\delta}} \\ \dot{\boldsymbol{\omega}} \end{bmatrix}}_{\dot{\mathbf{x}}} = \underbrace{\begin{bmatrix} 0 & I \\ -\boldsymbol{H}^{-1}L(\boldsymbol{p}) & -\boldsymbol{H}^{-1}\boldsymbol{D} \end{bmatrix}}_{A} \underbrace{\begin{bmatrix} \boldsymbol{\delta} \\ \boldsymbol{\omega} \end{bmatrix}}_{\mathbf{x}}, \qquad (6)$$

where $\boldsymbol{\omega}$ specifies the (dynamic) frequencies of the generators and $L(\boldsymbol{p})$ is a Laplacian or grounded-Laplacian matrix (see [16]) which is a function of the line susceptances and also the operating point. Specifically, the off-diagonal entries of matrix $L(\boldsymbol{p})$ are given by $L_{ij} = E_i^{ss}E_j^{ss}|\bar{Y}_{ij}|\sin\big(\delta_i^{ss} - \delta_j^{ss} - \bar{\phi}_{ij}\big)$ and the diagonal entries are chosen so that the row sums are zero. The small signal characteristics of interest are related to the solution of the linearized equation, and hence to the properties of state matrix A (e.g., its eigenvalues), see [17].

As a further step, properties of input-output channels in the network (e.g., control channels, critical disturbance responses) may be of interest. Formally, these input-output characteristics can be found by augmenting the linearized swing model ($\dot{\mathbf{x}} = A\mathbf{x}$) to incorporate an input and output. That is, the full system model $\dot{\mathbf{x}} = A\mathbf{x} + B\mathbf{u}$, $y = C\mathbf{x}$, where B and C are input and output matrices of interest, is considered. For example, we are interested in the channel performance between input as power injection at bus i and output as generator angle at bus j. In this case $B^T = \begin{bmatrix} 0 & \mathbf{e}_i \end{bmatrix}$, and $C = \begin{bmatrix} \mathbf{e}_j^T & 0 \end{bmatrix}$ where $\mathbf{e}_i$ is a vector with ith entry equal to 1 and other entries equal to 0. Input-output properties of the swing dynamics, particularly the finite and infinite zero structure, have been explored in [18], [19]. Both internal and input-output properties of the small-signal model are considered in the design here.

C. Performance Metrics

Metrics of small-signal and transient performance of the transmission network can be computed from the nonlinear and linear swing equations. Two performance metrics, which are concerned with the small-signal response, will be considered for optimization in this study:

1) **Disturbance Attenuation.** The attenuation of small disturbances, whether impulsive or persistent, is one natural metric for the network's dynamic performance. The damping of the network is one measure of disturbance attenuation and considered in this study. The damping is given by $\eta_S = \min\left(-\alpha_S/\sqrt{\alpha_S^2 + \beta_S^2}\right)$, where α_S and β_S are the real part and imaginary part of λ_S, which are the eigenvalues of the state matrix A. The minimization is over all the λ_S. It is worth noting that congestion or stress in the power network sometimes promotes low-frequency wide-area responses (i.e., the network becomes more "springy"), which may not always be directly related to the damping ratio. Alternative metrics, based on the two-norm of the impulse response, could be used to approximate disturbance attenuation. For simplicity, we do not consider these additional metrics here and focus on the damping, but note that the optimization formulation can be readily adapted to these other metrics.
2) **Control-Channel Performance.** The small-signal and transient performance is also reflected in the ability of deployed controllers to manage disturbances. In particular, it is important to characterize whether, and how effectively, existing control channels can be used to damp oscillations and transients. Characterization of

control channels for power-system fast dynamics is a complex problem of emerging interest, and much research is ongoing in this direction [20], [18], [21], [19], [22]. Several recent studies, which draw on the classical structural analysis of control systems, have argued for using the finite zeros of the control channels' transfer functions as indicators of performance. Here, we use the smallest damping ratio among the finite zeros as a metric for control-channel performance. Specifically, the metric is defined as $\eta_C = \min\left(-\alpha_C/\sqrt{\alpha_C^2+\beta_C^2}\right)$, where α_C and β_C are the real part and imaginary part of λ_C, which are the zeros of the system. The minimization is over all finite λ_C. The finite and infinite zeros of the full system model $\dot{\mathbf{x}} = A\mathbf{x} + B\mathbf{u}$, $y = C\mathbf{x}$ can be calculated via a generalized eigenvalue analysis:

$$\lambda_C = \text{eig}\left(\begin{bmatrix} A & B \\ C & 0 \end{bmatrix}, \begin{bmatrix} I & 0 \\ 0 & 0 \end{bmatrix}\right) \tag{7}$$

The transient stability margin of the system is another natural performance measure for the fast dynamics of the power network. Several specific definitions have been proposed for the transient stability margin, including the distance from the operating point to the boundary of the region of attraction [23], the distance from the power-transfer limit causing instability, and the critical fault clearing time for a specified set of contingencies [24]. However, each of these metrics is rather difficult to compute, which makes optimization of a transient stability metric challenging. For this reason, the transient stability margin is not considered further in this work.

Each of the defined metrics is dependent on the real power injections $\boldsymbol{p}$ affected by the demand response actions, which are the design variables in the optimization problem.

D. Optimization Problem

The optimization problem is to maximize a weighted combination of the two performance metrics by designing the real power injection vector $\boldsymbol{p}$. The full optimization problem is:

$$\max_{\boldsymbol{p}} \quad \gamma_S\eta_S + \gamma_C\eta_C \qquad \text{subject to} \tag{8a}$$

$$\eta_S = \min\left(\frac{-\alpha_S}{\sqrt{\alpha_S^2+\beta_S^2}}\right) \tag{8b}$$

$$\eta_C = \min\left(\frac{-\alpha_C}{\sqrt{\alpha_C^2+\beta_C^2}}\right) \tag{8c}$$

$$\alpha_S = \text{Re}\{\lambda_S\}, \beta_S = \text{Im}\{\lambda_S\} \tag{8d}$$

$$\lambda_S = \text{eig}(A) \tag{8e}$$

$$\alpha_C = \text{Re}\{\lambda_C\}, \beta_C = \text{Im}\{\lambda_C\} \tag{8f}$$

$$\lambda_C = \text{eig}\left(\begin{bmatrix} A & B \\ C & 0 \end{bmatrix}, \begin{bmatrix} I & 0 \\ 0 & 0 \end{bmatrix}\right) \tag{8g}$$

$$A = \begin{bmatrix} 0 & I \\ -\boldsymbol{H}^{-1}L(\boldsymbol{p}) & -\boldsymbol{H}^{-1}\boldsymbol{D} \end{bmatrix} \tag{8h}$$

$$L_{ij} = E_i^{ss}E_j^{ss}|\bar{Y}_{ij}|\sin\big(\delta_i^{ss} - \delta_j^{ss} - \bar{\phi}_{ij}\big), i \neq j \tag{8i}$$

$$L_{ii} = -\sum_{i\neq j} L_{ij} \tag{8j}$$

$$\bar{Y} = \mathcal{H}(Y, \boldsymbol{p}), \bar{\phi}_{ij} = \angle\bar{Y}_{ij} \tag{8k}$$

$$\mathcal{F}_i^P(\boldsymbol{\theta}, \boldsymbol{V}) = p_i \qquad \forall i \in \mathcal{N} \tag{8l}$$

$$\mathcal{F}_i^Q(\boldsymbol{\theta}, \boldsymbol{V}) = q_i \qquad \forall i \in \mathcal{N} \tag{8m}$$

$$\mathcal{G}_i^E(\boldsymbol{\theta}, \boldsymbol{V}) = E_i^{ss} \qquad \forall i \in \mathcal{S}_\text{G} \tag{8n}$$

$$\mathcal{G}_i^\delta(\boldsymbol{\theta}, \boldsymbol{V}) = \delta_i^{ss} \qquad \forall i \in \mathcal{S}_\text{G} \tag{8o}$$

$$\textstyle\sum_{i\in\mathcal{S}_\text{DR}} p_i = \varepsilon_0 \tag{8p}$$

$$p_i \cdot \mu_i = q_i \qquad \forall i \in \mathcal{S}_\text{PQ} \tag{8q}$$

$$p_i = p_i^0 \qquad \forall i \in \mathcal{S}_\text{PV}, \mathcal{S}_\text{PQ} \setminus \mathcal{S}_\text{DR} \tag{8r}$$

$$V_i = V_i^0 \qquad \forall i \in \mathcal{S}_\text{PV} \tag{8s}$$

$$V_\text{ref} = V_\text{ref}^0, \theta_\text{ref} = 0 \tag{8t}$$

$$\underline{\boldsymbol{p}} \leq \boldsymbol{p} \leq \overline{\boldsymbol{p}} \tag{8u}$$

$$\underline{\boldsymbol{q}} \leq \boldsymbol{q} \leq \overline{\boldsymbol{q}} \tag{8v}$$

$$\underline{\boldsymbol{V}} \leq \boldsymbol{V} \leq \overline{\boldsymbol{V}} \tag{8w}$$

Constraints (8b), (8d), (8e), and (8h) define η_S as the smallest damping ratio of the generator modes, while (8c), (8f), (8g), and (8h) define η_C as the damping ratio of the dominant zero. The diagonal and off-diagonal entries of Laplacian matrix in (8h) are shown in (8i) – (8k). Constraints (8l) and (8m) are the nonlinear AC power flow equations as defined in (1), (2). Constraints (8n) and (8o) are the nonlinear generator electromotive force (emf) equations as defined in (3), (4). Constraint (8p) forces the total demand responsive loads to remain constant, (8q) models loads as constant power factor loads, and (8r)–(8t) fixes the the real power injections of the PV buses and PQ buses without demand responsive loads, the voltage magnitudes of all buses with generators, and the voltage angle of the slack bus to their nominal values. The remaining constraints limit the design variables. We could also include constraints to compute/constrain the power flows but, for simplicity, we do not do that here.

IV. Solution Algorithm

The optimization problem is challenging, involving nonlinear, non-convex constraints. To solve the problem, we use *iterative linear programming*. The idea of iterative programming has been used to solve many kinds of optimization problems for the power system. Iterative linear programming is used to solve the basic AC-OPF problem [14, p. 371]. Moreover, it is used to solve the smallest singular value maximization problem in [12]. Reference [25] proposes an iterative quadratic programming approach to solve a multi-period AC-OPF problem including renewable generators and energy storage.

Iterative linear programming works as follows. At each iteration, we first linearize the cost and each of the nonlinear constraints about the current operating point. Then we solve the resulting linear program, where the new decision variables are the *changes* in the original decision variables. We bound the changes because the linearization is only valid in a small region around the original operating point. This yields an estimate of the solution for the original nonlinear program. For this solution estimate, the new operating point is computed

by solving the AC power flow equations. The process is then iterated: i.e., the nonlinear program is re-linearized around the new operating point to obtain a linear program, and this linear program is solved to get another estimate of the solution. The algorithm is continued until the solution estimate converges, either to the global optimal solution of the nonlinear problem or at least a local maxima. Before describing the iterative algorithm we derive the linear sensitivity of the damping ratio which is used to replace (8b)–(8k).

A. Linearization of the Nonlinear Constraints

The iterative linear programming approach requires approximation of the nonlinear optimization problem with a linear one, via linearization of the cost and constraints around the operating point for the current solution estimate. For the formulation given in Section IIID, the damping ratio computations as well as the power flow equations require linearization. The linearization of the power flow equations is standard, and hence details are omitted. Functions $f_i^P(\boldsymbol{\theta}, \boldsymbol{V})$, $f_i^Q(\boldsymbol{\theta}, \boldsymbol{V})$, $g_i^E(\boldsymbol{\theta}, \boldsymbol{V})$, and $g_i^\delta(\boldsymbol{\theta}, \boldsymbol{V})$ are used to denote the linearizations of constraints (8l)–(8o).

The linearization of the damping ratios can be derived using eigenvalue sensitivities. Specifically, the sensitivities of the eigenvalues to changes in the power flow variables can be determined, and subsequently the damping-ratio sensitivities can be determined. Let λ_i, u_i, and w_i be the eigenvalues, right eigenvectors, and left eigenvectors, respectively, of matrix $\mathcal{A}$, where the eigenvectors are normalized so that $w_i^T u_i = 1$. For any variable ξ that matrix $\mathcal{A}$ depends on, the derivative of λ_i with respect to ξ (i.e., the eigenvalue sensitivity [26]) can be found as

$$\frac{\partial \lambda_i}{\partial \xi} = w_i^T \frac{\partial \mathcal{A}}{\partial \xi} u_i. \tag{9}$$

In the disturbance attenuation problem, $\mathcal{A} = A$, which depends on $\boldsymbol{\delta}^{ss}$, $\boldsymbol{E}^{ss}$, and $\bar{Y}$. Hence, by using (9) and standard properties of derivatives, the change in the eigenvalue with the smallest damping ratio λ_S can be approximated as a linear function of δ_i^{ss} and E_i^{ss}, i.e.,

$$\Delta\lambda_S = \sum_{i \in \mathcal{S}_\mathrm{G}} \left(\left[w_S^T \frac{\partial A}{\partial E_i^{ss}} u_S \right] \Delta E_i^{ss} + \left[w_S^T \frac{\partial \mathcal{A}}{\partial \delta_i^{ss}} u_S \right] \Delta \delta_i^{ss} \right), \tag{10}$$

where u_S and w_S are the normalized right and left eigenvectors corresponding to the eigenvalue with smallest damping ratio, and where we have excluded the dependence on $\bar{Y}$ because it is typically very small. The entries in A exhibit simple algebraic dependences on the variables, which allow simple computation of the partial derivatives of A in the expression above; details are omitted.

Based on the eigenvalue sensitivity, the damping ratio sensitivity, which is also linear, is

$$\Delta\eta_S = \frac{(-\beta_S^2 \Delta\alpha_S + \alpha_S \beta_S \Delta\beta_S)}{(\alpha_S^2 + \beta_S^2)^{\frac{3}{2}}}, \tag{11}$$

where $\Delta\alpha_S = \mathrm{Re}\{\Delta\lambda_S\}$ and $\Delta\beta_S = \mathrm{Im}\{\Delta\lambda_S\}$.

The zero damping ratio can be linearized similarly.

B. Linear Program at Each Iteration

The linear program that is solved at each step of the iterative linear programming algorithm is as follows.

$$\max_{\Delta \boldsymbol{p}} \quad \gamma_S \Delta\eta_S + \gamma_C \Delta\eta_C \qquad \text{subject to} \tag{12a}$$

$$\Delta\eta_S = \frac{(-\beta_S^2 \Delta\alpha_S + \alpha_S \beta_S \Delta\beta_S)}{(\alpha_S^2 + \beta_S^2)^{\frac{3}{2}}} \tag{12b}$$

$$\Delta\eta_C = \frac{(-\beta_C^2 \Delta\alpha_C + \alpha_C \beta_C \Delta\beta_C)}{(\alpha_C^2 + \beta_C^2)^{\frac{3}{2}}} \tag{12c}$$

$$\Delta\lambda_S = \sum_{i \in \mathcal{S}_\mathrm{G}} \left(\left[w_S^T \frac{\partial A}{\partial E_i^{ss}} u_S \right] \Delta E_i^{ss} + \left[w_S^T \frac{\partial A}{\partial \delta_i^{ss}} u_S \right] \Delta \delta_i^{ss} \right) \tag{12d}$$

$$\Delta\lambda_C = \sum_{i \in \mathcal{S}_\mathrm{G}} \left(\left[\frac{w_C^T \begin{bmatrix} \frac{\partial A}{\partial E_i^{ss}} & 0 \\ 0 & 0 \end{bmatrix} u_C}{w_C^T \begin{bmatrix} I & 0 \\ 0 & 0 \end{bmatrix} u_C} \right] \Delta E_i^{ss} + \left[\frac{w_C^T \begin{bmatrix} \frac{\partial A}{\partial \delta_i^{ss}} & 0 \\ 0 & 0 \end{bmatrix} u_C}{w_C^T \begin{bmatrix} I & 0 \\ 0 & 0 \end{bmatrix} u_C} \right] \Delta \delta_i^{ss} \right) \tag{12e}$$

$$\Delta\alpha_S = \mathrm{Re}\{\Delta\lambda_S\}, \Delta\beta_S = \mathrm{Im}\{\Delta\lambda_S\} \tag{12f}$$

$$\Delta\alpha_C = \mathrm{Re}\{\Delta\lambda_C\}, \Delta\beta_C = \mathrm{Im}\{\Delta\lambda_C\} \tag{12g}$$

$$f_i^P(\boldsymbol{\theta}, \boldsymbol{V}) = \Delta p_i \qquad \forall i \in \mathcal{N} \tag{12h}$$

$$f_i^Q(\boldsymbol{\theta}, \boldsymbol{V}) = \Delta q_i \qquad \forall i \in \mathcal{N} \tag{12i}$$

$$g_i^E(\boldsymbol{\theta}, \boldsymbol{V}) = \Delta E_i^{ss} \qquad \forall i \in \mathcal{S}_\mathrm{G} \tag{12j}$$

$$g_i^\delta(\boldsymbol{\theta}, \boldsymbol{V}) = \Delta \delta_i^{ss} \qquad \forall i \in \mathcal{S}_\mathrm{G} \tag{12k}$$

$$\textstyle\sum_{i \in \mathcal{S}_\mathrm{DR}} \Delta p_i = 0 \tag{12l}$$

$$\Delta p_i \cdot \mu_i = \Delta q_i \qquad \forall i \in \mathcal{S}_\mathrm{PQ} \tag{12m}$$

$$\Delta p_i = 0 \qquad \forall i \in \mathcal{S}_\mathrm{PV}, \mathcal{S}_\mathrm{PQ} \setminus \mathcal{S}_\mathrm{DR} \tag{12n}$$

$$\Delta V_i = 0 \qquad \forall i \in \mathcal{S}_\mathrm{PV} \tag{12o}$$

$$\Delta V_\mathrm{ref} = 0, \Delta\theta_\mathrm{ref} = 0 \tag{12p}$$

$$\underline{\boldsymbol{p}} \le \boldsymbol{p}^0 + \Delta p \le \overline{\boldsymbol{p}} \tag{12q}$$

$$\underline{\boldsymbol{q}} \le \boldsymbol{q}^0 + \Delta q \le \overline{\boldsymbol{q}} \tag{12r}$$

$$\underline{\boldsymbol{V}} \le \boldsymbol{V}^0 + \Delta V \le \overline{\boldsymbol{V}} \tag{12s}$$

$$\Delta\eta_S \le \overline{\Delta\eta} \tag{12t}$$

$$\Delta\eta_C \le \overline{\Delta\eta} \tag{12u}$$

where (12b)–(12g) are the linearizations of the damping ratio constraints (8b)–(8k), and (12h)–(12s) are the linearizations of (8l)–(8w). Notice here that the linearization of the dominant zero damping ratio depends on a generalized eigenvector analysis of the input-to-output system; details have been omitted to simplify the presentation, see [27] for background on the analysis. To ensure the accuracy of the linearization, (12t) and (12u) are added to limit the step size of $\Delta\eta$, where $\overline{\Delta\eta}$ is a user-chosen parameter. After obtaining the solution to the linear program, $\boldsymbol{p}^0$ is updated by adding $\boldsymbol{\Delta p}^*$. Then, $\boldsymbol{V}^0$,

$\boldsymbol{\theta}^0$, $\boldsymbol{q}^{\mathbf{0}}$, $\boldsymbol{E}^{\boldsymbol{ss0}}$ and $\boldsymbol{\delta}^{\boldsymbol{ss0}}$ are updated by re-solving the AC power flow and generator dynamics equations (1)–(4). The new smallest damping ratio of the generator modes and zeros ($\eta_S,\ \eta_C$), and eigenvalues ($\lambda_S,\ \lambda_C$) are re-computed at the new operating point. The algorithm is terminated when $\Delta\eta_S$ and $\Delta\eta_C$ both go below a small threshold (here, we use 10^{-4}). Note that for practical implementation of the algorithm, we would need to compute/constrain the power flows. These constraints can be easily incorporated and do not increase the complexity of the problem.

V. Exploratory characterization of the optimum considering a simplified model

Analytical characterization of the power system's behavior for the optimal design is appealing, for several reasons [28], [29]. First, such characterizations may provide a path for finding or approximating the optimal design analytically. Also, these characterizations may enable selection of high-performing designs even if the optimal design is hard to compute, or the model is subject to parametric uncertainties. In a similar vein, the characterizations may yield simple rubrics for tuning demand response actions and other load-side resources.

Here, we pursue an exploratory characterization of the system's behavior at the optimum, based on a simplified cost metric and model. Specifically, let us consider only the smallest damping of the generator modes η_S as the cost, and assume the system is at an optimum load design $\boldsymbol{p}^*$ that maximizes the smallest damping of system. Let λ_S be the mode of the system with the smallest damping ratio η_S. The simplified optimization problem (compared to (8a)) which only captures the smallest damping of the network can be written as:

$$\boldsymbol{p}^* = \max_{\boldsymbol{p}}(\eta_S) \tag{13}$$

To characterize the optimum, we form the Lagrangian as $\Phi = \eta_S + a(\sum_i p_i - \varepsilon_0) + \sum_i b_i(\underline{p}_i - p_i + \tau_i^2) + \sum_i c_i(p_i - \overline{p}_i + \nu_i^2)$, where a, b_i, and c_i are the Lagrangian multipliers, and τ_i and ν_i are the slack variables, $\forall i \in \mathcal{S}_{\mathrm{DR}}$. Based on Karush-Kuhn-Tucker conditions, at the optimum, the derivative of Φ with respect to each variable (a, b_i, c_i, τ_i, and ν_i) is zero. By assuming that the optimum is not on the boundary ($\tau_i \neq 0$ and $\nu_i \neq 0$) we get the following equations which can be solved to find the optimum:

$$\frac{\partial \eta_S}{\partial p_i} + a = 0 \tag{14}$$

$$\sum_i p_i - \varepsilon_0 = 0 \tag{15}$$

$$\underline{p}_i - p_i + \tau_i^2 = 0 \tag{16}$$

$$p_i - \overline{p}_i + \nu_i^2 = 0 \tag{17}$$

Let us simplify (14). To do so, we can use the eigenvalue sensitivity formula (9) and the sensitivity of the damping ratio (11) to obtain

$$-\beta \operatorname{Re}\left(w_S^T \frac{\partial A}{\partial p_i} u_S\right) + \alpha \operatorname{Im}\left(w_S^T \frac{\partial A}{\partial p_i} u_S\right) = \bar{a}. \tag{18}$$

If the system is at an optimum design, the left side of (18) should be identical for all i. Conceptually, the equation shows that the optimal design serves to equalize the sensitivity of the damping ratio to each designable load.

We next simplify the left side of (18), so as to give a relationship among the parameters of the model at the optimum. To do so, let us consider a simplified dynamical model which helps to simplify the calculation of $\frac{\partial A}{\partial p_i}$. In this simplified model, the loads are modeled as fixed power and the voltage magnitude at load buses are assumed fixed similar to generator buses. By using these assumptions and ignoring the transmission conductance in the power system, the classical nonlinear swing dynamics model, upon applying standard approximations used in the formal analysis of transients, takes the form:

$$H_i \ddot{\delta}_i = p_i - D_i \dot{\delta}_i - \sum_{j \neq i} E_i^{ss} E_j^{ss} B_{ij} \sin(\delta_i - \delta_j). \tag{19}$$

To simplify computation of the partial derivatives, a simplified lossless linear power-flow model is used to compute the change in the operating point due to the demand response actions. By assuming that the transient reactance is small, the steady-state phase angles $\boldsymbol{\theta}$ are an equilibrium solution for the angles $\boldsymbol{\delta}^{ss}$. Also, V_i is equivalent to E_i^{ss} in the swing-dynamics equation. With this assumption, the steady-state phase angles at the buses upon deployment of the demand response can be computed as $\boldsymbol{\theta} = \boldsymbol{\theta}^0 + \widehat{B}^{-1}(\boldsymbol{p} - \boldsymbol{p}^0)$, where the matrix $\widehat{B}$ contains "effective" line susceptances based on a linearization of the power flow equations at the nominal operating point. We notice here that the design variable $\boldsymbol{p}$ enters the equation as a driving term. This set of nonlinear differential-algebraic equations can be linearized around its operating point resulting in a system of the form (6), where $L(\boldsymbol{p}) = \widehat{B}_{gg} - \widehat{B}_{gl}\widehat{B}_{lg}^{-1}\widehat{B}_{lg}$. The off-diagonal entries of $\widehat{B}$ are given by $\widehat{B}_{ij} = V_i V_j B_{ij} \cos(\theta_i - \theta_j)$ and the diagonal entries are chosen so that the row sums are zero. In this expression, the matrices $\widehat{B}_{gg}$, $\widehat{B}_{gl}$, $\widehat{B}_{lg}$, and $\widehat{B}_{ll}$ are partitions of $\widehat{B}$ commensurate with the generator and load buses.

Given these assumptions, we have

$$\frac{\partial A}{\partial p_i} = \begin{bmatrix} 0 & 0 \\ -\frac{\partial L(\boldsymbol{p})}{\partial p_i} & 0 \end{bmatrix}, \tag{20}$$

where

$$\begin{aligned} \frac{\partial L(\boldsymbol{p})}{\partial p_i} =& \sum_j \frac{\partial \widehat{B}_{gg}}{\partial \theta_j}\frac{\partial \theta_j}{\partial p_i} - \sum_j \frac{\partial \widehat{B}_{gl}}{\partial \theta_j}\frac{\partial \theta_j}{\partial p_i}\widehat{B}_{ll}^{-1}\widehat{B}_{lg} \\ & - \widehat{B}_{gl}\widehat{B}_{ll}^{-1}\sum_j \frac{\partial \widehat{B}_{lg}}{\partial \theta_j}\frac{\partial \theta_j}{\partial p_i} \\ & + \widehat{B}_{gl}\widehat{B}_{ll}^{-1}\sum_j \frac{\partial \widehat{B}_{ll}}{\partial \theta_j}\frac{\partial \theta_j}{\partial p_i}\widehat{B}_{ll}^{-1}\widehat{B}_{lg}. \end{aligned} \tag{21}$$

The terms in the above expression can be found explicitly, as follows:

$$\frac{\partial \theta_j}{\partial p_i} = \left[\widehat{B}^{-1}\right]_{j,i} \tag{22}$$

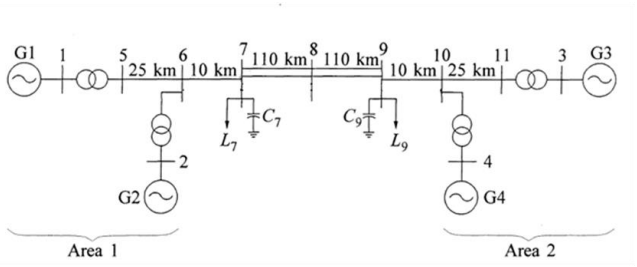

Fig. 2. Kundur's two-area 11-bus test system [17].

$$\left[\frac{\partial \widehat{B}}{\partial \theta_j}\right]_{r,s} = 0 \qquad r \neq j, s \neq j \tag{23}$$

$$\left[\frac{\partial \widehat{B}}{\partial \theta_j}\right]_{r,s} = -V_r V_s B_{r,s} \sin(\theta_r - \theta_s) \qquad r = j, s \neq j \tag{24}$$

$$\left[\frac{\partial \widehat{B}}{\partial \theta_j}\right]_{r,s} = V_r V_s B_{r,s} \sin(\theta_r - \theta_s) \qquad r \neq j, s = j \tag{25}$$

$$\left[\frac{\partial \widehat{B}}{\partial \theta_j}\right]_{r,s} = -\sum_{q \neq j} V_j V_q B_{j,q} \sin(\theta_j - \theta_q) \qquad r = j, s = j \tag{26}$$

Plugging (22)–(26) into (18), one recovers a set of relationships among the parameters of the power system model at the optimum, albeit rather complex ones. Specifically, the relationships indicate that certain functions of the eigenvector associated with the worst-damped mode, the network matrix, and the operating point are identical at the optimum, provided that the optimum is not on the boundaries of the power constraints. We believe that these relationships may a starting point toward simple tuning schemes for demand response actions, because they may indicate whether a load should be increased or decreased toward achieving the optimum solution, and also how sensitive the damping ratio is to a load change. Much remains to be done to translate this formal analysis to practical tuning algorithms; we hope to pursue this in future work.

VI. Case Studies and Discussion

We applied the iterative algorithm introduced in Section IV to Kundur's two-area 11-bus test system shown in Fig. 2. We choose generator 1 as the reference generator. The inertias and dampings of the remaining generators are $H_{2-4} = [58.5\ 55.6\ 55.6]$ p.u. and $D_{2-4} = [210\ 140\ 70]$ p.u.. We use MATPOWER [30] to solve the power flow equations. The solution for the nominal system is shown in Table I and the three electromechanical eigenvalues, damping ratios, and swing profiles are shown in Table II. The swing profile indicates which two generators are involved in the intermachine mode corresponding to the eigenvalue as determined by the participation factors [31, p. 229]. The zeros of the transfer function between power injection at bus 2 (input) and generator angle at bus 4 (output) are $-0.6298 \pm 6.2198j$.

TABLE I
Power flow solution of the nominal System

Bus	p^0 (MW)	q^0 (MVar)	V^0 (p.u.)
1	710	141	1.030
2	700	123	1.010
3	719	106	1.030
4	700	33	1.010
7	-967	-100	0.994
9	-1767	-100	1.021

TABLE II
Eigenvalues of the nominal system

Eigenvalues (rad/s)	Damping	Swing Profile
$-0.4462 \pm 6.7715j$	6.5747	$3 \leftrightarrow 4$
$-0.4981 \pm 2.7430j$	17.8685	$3 \leftrightarrow 4$
$-0.8978 \pm 5.4766j$	16.1771	$2 \leftrightarrow 3$

We first investigate the influence of demand response on the smallest damping ratio of the generator modes. We set $\gamma_S = 1, \gamma_C = 0, \bar{\eta} = 0.01$. The solution to (12) is given in Table III. By increasing the power consumption at bus 7 and decreasing that at bus 9, the smallest damping ratio of generator modes increases from 6.5747 to 6.9186.

To verify the results, we compare the solution of the iterative approach to that of a brute force approach. We compute the smallest damping ratio of the generator modes for all possible loading patterns with a 1 MW mesh size. Figure 3 shows the smallest damping ratio as a function of the real power injection at bus 7 p_7 (based on (8p), $p_9 = -2734 - p_7$ MW). When p_7 is larger than -905 MW, the Kundur system does not have power flow solution; when p_7 is smaller than -1680 MW, the Kundur system is unstable since it has an eigenvalue in the right half plane. The maximum smallest damping ratio is 6.9186 when $p_7^* = -1680$ MW, $p_9^* = -1054$ MW. The solution of iterative approach, shown in Table III, is very near to the optimum determined by the brute force method. Figure 4 shows the impulse response of the nominal case and the maximum smallest damping ratio case. As shown, the energy of the impulse response in optimum case is less than that in the nominal case.

Table IV shows how the optimal power injection at bus 7 and the tie line (branch $8-9$) flow change for different generator 4 dampings. hen area 2 becomes more damped, the optimal power transfer from area 1 to area 2 reduces and eventually changes direction. From this example we can see that when real power generation at PV buses is fixed, if one area in the system is more damped than the other, the smallest damping ratio of the generator modes can be increased by increasing the power flow from the less damped area to the more damped area.

We next compare the improvement made by demand response along to that possible with generation redispatch and

TABLE III
POWER FLOW SOLUTION MAXIMIZING THE SMALLEST DAMPING RATIO VIA DEMAND RESPONSE ALONE

Bus	p^* (MW)	q^* (MVar)	V^* (p.u.)
1	697	154	1.030
2	700	163	1.010
3	719	47	1.030
4	700	-107	1.010
7	-1679	-174	0.982
9	-1055	-59	1.063

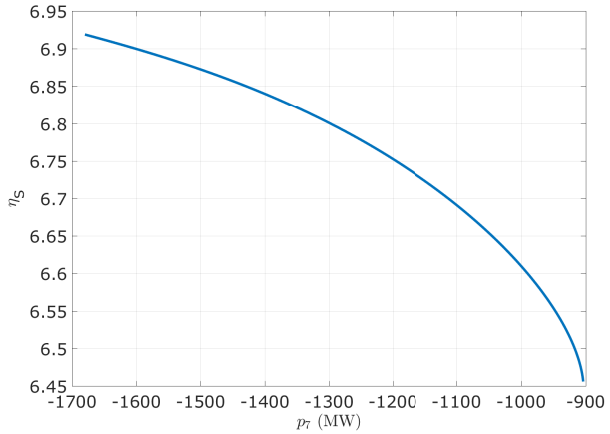

Fig. 3. Smallest damping ratio of the generator modes as a function of the power injection at bus 7.

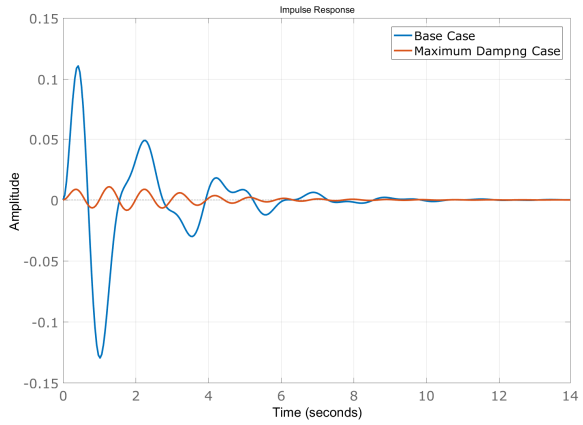

Fig. 4. Impulse response across the tie line for the nominal system (base case) and the system in which the smallest damping ratio of the generator modes is maximized via demand response alone (maximum damping case).

TABLE IV
OPTIMAL POWER INJECTIONS AT BUS 7 AND TIE LINE FLOWS FOR DIFFERENT GENERATOR 4 DAMPINGS

D_4 (p.u.)	70	140	210	250	350
p_7^* (MW)	-1680	-1581	-1403	-1320	-905
tie line flow (MW)	-324	-230	-56	27	473

voltage regulation. We use the iterative approach to determine the optimal operating point for different choices of decision variables, given in Table V. Note that generator reactive power is always a decision variable.

TABLE V
DECISION VARIABLES FOR EACH CASE

Case	1	2	3	4	5	6	7
generator real power		✓	✓		✓	✓	
load real/reactive power	✓		✓	✓		✓	
voltage magnitudes at PV buses				✓	✓	✓	✓

Table VI summarizes the results by listing the generation at buses $1-4$, load at buses 7 and 9, voltage magnitudes, smallest damping ratio (η_S) and percentage improvement (Δ) for each case. As shown, the greatest improvement happens when we change generation, load, and voltage magnitudes together. Generation re-dispatch alone improves the smallest damping ratio the most (25.5%), followed by voltage regulation alone (13.1%). Demand response alone does not improve the smallest damping ratio as much (5.2%); however, in practice, generators may not be able to fully react as quickly as loads.

TABLE VI
OPTIMAL OPERATING POINT, SMALLEST DAMPING RATIO, AND PERCENTAGE IMPROVEMENT FOR EACH CASE

Case	1	2	3	4	5	6	7
p^* (MW)	$\begin{bmatrix}697\\700\\719\\719\\1679\\1055\end{bmatrix}$	$\begin{bmatrix}639\\824\\94\\1270\\967\\1767\end{bmatrix}$	$\begin{bmatrix}350\\1134\\68\\1241\\1758\\976\end{bmatrix}$	$\begin{bmatrix}696\\700\\719\\700\\1551\\1183\end{bmatrix}$	$\begin{bmatrix}368\\1075\\107\\1270\\967\\1767\end{bmatrix}$	$\begin{bmatrix}384\\1147\\11\\1269\\1094\\1640\end{bmatrix}$	$\begin{bmatrix}697\\700\\719\\700\\967\\1767\end{bmatrix}$
V^* (p.u.)	$\begin{bmatrix}1.030\\1.010\\1.030\\1.010\\0.990\\1.020\end{bmatrix}$	$\begin{bmatrix}1.030\\1.010\\1.030\\1.010\\0.976\\1.011\end{bmatrix}$	$\begin{bmatrix}1.030\\1.010\\1.030\\1.010\\0.983\\1.079\end{bmatrix}$	$\begin{bmatrix}1.070\\0.922\\1.015\\0.903\\0.926\\0.964\end{bmatrix}$	$\begin{bmatrix}1.100\\1.100\\0.937\\0.915\\1.070\\0.900\end{bmatrix}$	$\begin{bmatrix}1.088\\1.074\\0.906\\0.921\\1.045\\0.916\end{bmatrix}$	$\begin{bmatrix}1.100\\1.100\\1.062\\0.900\\1.084\\0.947\end{bmatrix}$
η_S	6.92	8.25	8.62	7.57	11.03	12.87	7.44
Δ (%)	5.2	25.5	31.2	13.2	67.8	95.8	13.1

We next add the smallest damping ratio of the zeros into the cost function. We also change the damping of generators to $D_{2-4} = [210\ 140\ 210]$ p.u.. Figure 5 shows the smallest damping ratio of the generator modes and zeros as a function of p_7. The solutions from the iterative approach under different weighting factors are given in Table VII. As shown, the iterative algorithm produces the same results as the brute force method.

TABLE VII
OPTIMAL SOLUTIONS TO (12) UNDER DIFFERENT WEIGHTING FACTORS

$[\gamma_S\ \gamma_C]$	[1 0]	[0 1]	[25 1]
p_7^* (MW)	-1402	-1680	-1490
η_S	12.06	12.01	12.06
η_C	10.48	15.56	10.66

In this example, the maximum smallest damping ratio of the generator modes is 12.06 when $p_7^* = -1402$ MW. To check the statement in Section V that the value of $\bar{a}$ in (18)

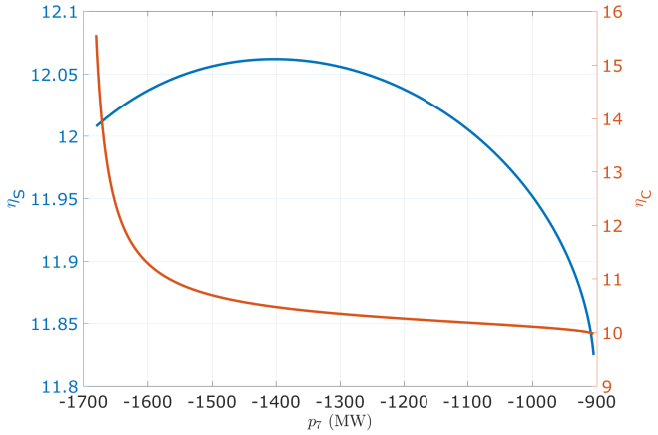

Fig. 5. Smallest damping ratio of the generator modes and zeros as a function of the power injection at bus 7 (using different generator dampings than in Fig. 3).

is identical for different PQ buses, Table VIII shows the value of $\bar{a}_7$ and $\bar{a}_9$ for different power injections at bus 7. They are the same at the optimum.

TABLE VIII
$\bar{a}_7$ AND $\bar{a}_9$ UNDER DIFFERENT p_7

p_7 (MW)	$\bar{a}_7(\times 10^{-3})$	$\bar{a}_9(\times 10^{-3})$	$\bar{a}_7 - \bar{a}_9(\times 10^{-3})$
-967	-7.4	-49.7	42.3
-1100	-5.0	-23.6	18.6
-1200	-4.2	-15.2	11.0
-1300	-3.6	-8.9	5.3
-1402	-3.1	-3.1	0
-1500	-2.7	2.7	-5.4
-1600	-2.5	9.8	-12.3

VII. Conclusions and Future Work

This paper has presented methods to improve power system small-signal and transient performance by using demand response. The smallest damping ratio of the generator modes and the smallest damping ratio of the zeros serve as measures of the small-signal stability and the control-channel performance. Specially, we formulated an optimization model that uses the linear combination of these two indicators as the cost function. The solution to the problem is obtained by using the linear eigenvalue sensitivity and applying an iterative linear programming algorithm. We applied the algorithm to a Kundur two-area 11-bus test system and benchmarked its performance against a brute force approach.

The test case results show that demand response actions which shift load between buses, while keeping the total load constant, can improve small-signal stability and controller performance. The loading pattern obtained by the iterative algorithm is near to the actual maximum determined by the brute force method. Moreover, the damping sensitivity with respect to the demand response power consumption is identical for all demand response buses at the optimal point. For this small system, demand response does not significantly improve the stability indicators as compared to generation re-dispatch and voltage regulation. However, there are more generator buses than demand buses in this example, which is atypical, and, in practice, ramp limits would prevent the generators from responding fast.

We suspect that use of demand response would be advantageous in short time horizons and in larger scale power systems. This needs to be verified by applying the iterative algorithm on larger scale power systems and taking into consideration the ramp limits of the generators in the optimization problem. Future work also includes including transient stability margins in the optimization formulation.

References

[1] L. Wang, F. Howell, P. Kundur, C. Chung, and W. Xu, "A tool for small-signal security assessment of power systems," in *Power Industry Computer Applications, 2001. PICA 2001. Innovative Computing for Power-Electric Energy Meets the Market. 22nd IEEE Power Engineering Society International Conference on*. IEEE, 2001, pp. 246–252.

[2] L. Wang and C. Chung, "Increasing power transfer limits at interfaces constrained by small-signal stability," in *Power Engineering Society Winter Meeting, 2002. IEEE*, vol. 2. IEEE, 2002, pp. 1184–1187.

[3] C. Chung, L. Wang, F. Howell, and P. Kundur, "Generation rescheduling methods to improve power transfer capability constrained by small-signal stability," *IEEE Transactions on Power Systems*, vol. 19, no. 1, pp. 524–530, 2004.

[4] S. Mendoza-Armenta and I. Dobson, "Applying a formula for generator redispatch to damp interarea oscillations using synchrophasors," *IEEE Transactions on Power Systems*, vol. 31, no. 4, pp. 3119–3128, 2016.

[5] ——, "A formula for damping interarea oscillations with generator redispatch," in *Proceedings of the IREP Symposium on Bulk Power System Dynamics and Control*, 2013.

[6] L. Yazdani and M. R. Aghamohammadi, "Damping inter-area oscillation by generation rescheduling based on wide-area measurement information," *International Journal of Electrical Power & Energy Systems*, vol. 67, pp. 138–151, 2015.

[7] Z. Huang, N. Zhou, F. Tuffner, Y. Chen, D. Trudnowski, W. Mittelstadt, J. Hauer, and J. Dagle, "Improving small signal stability through operating point adjustment," in *Power and Energy Society General Meeting, 2010 IEEE*. IEEE, 2010, pp. 1–8.

[8] A. L. Bettiol, L. Wehenkel, and M. Pavella, "Transient stability-constrained maximum allowable transfer," *IEEE Transactions on Power Systems*, vol. 14, no. 2, pp. 654–659, 1999.

[9] D. S. Callaway and I. A. Hiskens, "Achieving controllability of electric loads," *Proceedings of the IEEE*, vol. 99, no. 1, pp. 184–199, 2011.

[10] J. Short, D. Infield, and L. Freris, "Stabilization of grid frequency through dynamic demand control," *IEEE Transactions on Power Systems*, vol. 22, no. 3, pp. 1284–1293, 2007.

[11] E. Vrettos and G. Andersson, "Combined load frequency control and active distribution network management with controllable loads," *Proceedings of SmartGridComm*, 2013.

[12] M. Yao, J. Mathieu, and D. Molzahn, "Using demand response to improve power system voltage stability margins," in *Proceedings of IEEE PowerTech*, 2017.

[13] W. Hu, C. Wang, Z. Chen, and B. Bak-Jensen, "Power system transient stability improvement using demand side management in competitive electricity markets," in *European Energy Market (EEM), 2012 9th International Conference on the*. IEEE, 2012, pp. 1–8.

[14] A. J. Wood and B. F. Wollenberg, *Power Generation, Operation, and Control*. John Wiley & Sons, 2012.

[15] A. F. Paul M. Anderson, *Power system control and stability (second edition)*. Piscataway,NJ:IEEE Press, 2003.

[16] C. L. DeMarco and J. Wassner, "A generalized eigenvalue perturbation approach to coherency," in *Control Applications, 1995., Proceedings of the 4th IEEE Conference on*. IEEE, 1995, pp. 611–617.

[17] P. Kundur, N. J. Balu, and M. G. Lauby, *Power system stability and control*. McGraw-hill New York, 1994, vol. 7.

[18] K. Koorehdavoudi, M. Hatami, S. Roy, V. Venkatasubramanian, P. Panciatici, F. Xavier, and J. A. Torres, "Input-output characteristics of the power transmission network's swing dynamics," in *Decision and Control (CDC), 2016 IEEE 55th Conference on*. IEEE, 2016, pp. 1846–1852.

[19] K. Koorehdavoudi, S. Roy, T. Prevost, F. Xavier, P. Panciatici, and V. Venkatasubramanian, "Input-output properties of the swing dynamics for power transmission networks with hvdc modulation," in *Proceedings of the 20th IFAC World Congress*, 2017.

[20] N. Martins, H. J. Pinto, and L. T. Lima, "Efficient methods for finding transfer function zeros of power systems," *IEEE Transactions on Power Systems*, vol. 7, no. 3, pp. 1350–1361, 1992.

[21] J. A. Torres and S. Roy, "A two-layer transformation for characterizing the zeros of a network input-output dynamics," in *Decision and Control (CDC), 2015 IEEE 54th Annual Conference on*. IEEE, 2015, pp. 902–907.

[22] K. Koorehdavoudi, S. Roy, J. A. Torres, and M. Xue, "Interactions among control channels in dynamical networks," in *2017 IEEE 56th Conference on Decision and Control (CDC)*. IEEE, 2017.

[23] P. Varaiya, F. F. Wu, and R.-L. Chen, "Direct methods for transient stability analysis of power systems: Recent results," *Proceedings of the IEEE*, vol. 73, no. 12, pp. 1703–1715, 1985.

[24] Y. Zhang, L. Wehenkel, P. Rousseaux, and M. Pavella, "Sime: A hybrid approach to fast transient stability assessment and contingency selection," *International Journal of Electrical Power & Energy Systems*, vol. 19, no. 3, pp. 195–208, 1997.

[25] J. F. Marley, D. K. Molzahn, and I. A. Hiskens, "Solving multiperiod opf problems using an ac-qp algorithm initialized with an socp relaxation," *IEEE Transactions on Power Systems*, 2016.

[26] T. Smed, "Feasible eigenvalue sensitivity for large power systems," *IEEE Trans. Power Syst.*, vol. 8, no. 2, pp. 555–563, 1993.

[27] H. J. P. Martins, Nelson and L. T. Lima, "Efficient methods for finding transfer function zeros of power systems," *IEEE Transactions on Power Systems*, vol. 7, no. 3, pp. 1350–1361, 1992.

[28] J. Abad Torres, S. Roy, and Y. Wan, "Sparse resource allocation for linear network spread dynamics," *IEEE Transactions on Automatic Control*, vol. 62, no. 4, pp. 1714–1728, 2017.

[29] J. Abad Torres, S. Roy, and S. Rausch, "Sparse linear and nonlinear controls for network spread processes," *American Control Conference (ACC)*, pp. 3372–3377, 2016.

[30] R. Zimmerman, C. Murillo-Sanchez, and R. Thomas, "MATPOWER: Steady-state operations, planning, and analysis tools for power systems research and education," *IEEE Trans. Power Syst.*, vol. 26, no. 1, pp. 12–19, Feb 2011.

[31] P. W. Sauer and M. Pai, *Power system dynamics and stability*. Stipes, 1997.